

Interaction of galactic wind with halo gas and the origin of multiphase extraplanar material

Mahavir Sharma^{1*}, Biman B. Nath^{1†}, Indranil Chattopadhyay² and Yuri Shchekinov^{3‡}

¹ Raman Research Institute, Sadashivanagar, Bangalore 560080, India

² Aryabhata Research Institute of Observational Sciences, Manora Peak, Nainital 263129, India

³ Department of Physics, Southern Federal University, Rostov on Don 344090, Russia

Submitted ——— ; Accepted ——— ; In original form ———

ABSTRACT

We study the interaction of galactic wind with hot halo gas with hydrodynamical simulation. We find that the outcome of this interaction depends crucially on the wind injection density and velocity. If the cooling time of the gas in the interaction zone between the wind and halo gas exceeds the dynamical time of the wind, then a significant amount of warm-hot (10^5 – 10^6 K) gas is produced in the interaction zone, which we identify as warm circum-galactic medium (CGM) that can be detected through OVI absorption. If the cooling time is shorter, then the gas in interaction zone fragments into cold clouds. The clouds which form on the side walls of the wind cone, arising from eddies formed due to relative motion between the wind and halo gas, and can resemble high velocity clouds (HVCs). For high injection speed and density, the clouds formed in the thin shell on top of the wind are driven by ram pressure of the steady wind and represent the case of cold/warm clouds observed to be embedded in galactic outflows. We therefore find that the interaction between wind and halo gas can explain the occurrence of a variety of phenomena ranging from HVCs, outflowing clouds and warm CGM, depending on the combination of wind injection speed and density. We show the different regimes in the parameter space of wind speed and density, and discuss the implications in the context of star formation rates of galaxies.

Key words: galaxies : evolution – galaxies : haloes – galaxies : starburst – X-rays : galaxies

1 INTRODUCTION

Disk galaxies contain a substantial amount of baryonic matter outside the disk, and this extra-planar material has become an important problem to study for a number of reasons. Theoretically, since the pioneering papers by Spitzer (1956) and Pickelner & Shklovsky (1958) that invoked the presence of a high pressure ‘coronal’ gas outside the disk, its existence has been debated. Early works on galaxy formation suggested that the collapse of halos should lead to shock heated gas in the halo. However, various physical processes during the galactic evolution, such as star formation, galaxy mergers and stripping by intergalactic medium (IGM) would have played a significant role in shaping the extra-planar material that is observed today. Recent observations have detected this extra-planar gas in HI (e.g. Swaters et al. 1997) in H α (Rossa et al. 2004; Voigtländer et al. 2013) and in X-rays (Wang 2001; Strickland et al. 2004). The extra-planar gas, and its different phases, appear in the literature under different names, a few of which are listed below.

Hot halo gas: In the standard cold dark matter scenario of structure formation in the universe, baryonic gas falls into dark matter potentials and gets heated to the virial temperature (Silk 1977; White & Rees 1978; White & Frenk 1991). The gas then cools radiatively, and if the temperature is such that the cooling is rapid (for $T \leq 10^6$ K), for the case of low mass galaxies, then no accretion shock develops outside the evolving disk, and most of the halo gas remains at a temperature lower than the virial temperature (Binney 1977; Birnboim & Dekel 2003). This scenario of ‘cold accretion’ for low mass galaxies has received some observational support in recent years (e.g., Smith et al 2008). In massive galaxies, the hot halo gas is believed to cool slowly, and eventually form warm (10^4 K) clouds embedded in a large scale hot corona. These clouds could fall down on the disk in the form of high velocity clouds (e.g. Maller & Bullock 2004; Kauffmann et al. 2006). Numerical simulations have also shown that disk galaxies to be embedded in a hot gaseous halo (Toft et al 2002; Keres et al 2005), and that the X-ray luminosity of the halo gas should scale with galactic mass. However this hypothetical hot halo gas is yet to be observed (e.g. Rasmussen et al. 2009, and references therein), and the observations of the extraplanar gas so far have been limited to regions close to the disk and bulge, or around active star forming regions (e.g. Wang 2007). Moreover, if the halo does contain a

* mahavir@rri.res.in

† biman@rri.res.in

‡ yus@sfedu.ru

large amount of gas, it could potentially explain the missing baryon problem, which states that more than 80% of the baryons are unaccounted for by collapsed gas and stars in galaxies (Fukugita et al. 1998; Anderson & Bregman 2010).

Galactic wind: The subsequent evolution of the halo gas is thought to be governed both by the inflow of gas from the IGM and energy injection processes in the disk. Many star forming galaxies have been observed to contain a large amount of outflowing gas. The early observations of outflowing gas in M82 led to the development of Parker-type steady winds with energy and mass injection from supernovae (SNe) (Burke 1968; Johnson & Axford 1971; Chevalier & Clegg 1985). These calculations showed that fast steady winds with speeds exceeding 1000 km s^{-1} are possible to generate from the central regions of M82-type starburst galaxies. Wang (1995) explored steady wind solution with radiative cooling and showed that OVI emission in halos can arise from thermally unstable outflows. Numerical simulations have also been carried out in this regard (e.g. Suchkov et al. 1994; Mac Low & Ferrara 1999). Recently Sharma & Nath (2013) studied steady galactic winds from dark matter halos (with Navarro-Frenk-White (NFW) density profile (Navarro et al. 1997)) and found that SNe can drive outflows from dwarf galaxies, and active galactic nuclei (AGN) become important in driving outflows from massive galaxies, e.g., ultra-luminous infrared galaxies (ULIRGs). They also found that winds from intermediate sized galaxies which are in a quiescent mode of star formation (e.g. Milky Way) can not escape the halo. As a consequence of this, one can explain the observed trend of the stellar to halo mass ratio.

Outflowing cold/warm clouds: The outflowing gas is often observed to contain a clumpy component that contains neutral or partially ionized atoms, at 10^4 K (e.g. Martin 2005). In starbursts such as M82, molecular clouds and filaments have also been observed in the outflowing gas (Veilleux et al. 2009). The dynamics of these clouds offer useful clues to the formation and evolution of the outflowing gas, and recently have been used to discuss various physical processes that drives these clouds. Martin (2005) and Murray et al. (2005) suggested that radiation pressure on dust grains embedded in these clouds may play an important role in their dynamics (see also, Sharma et al. 2011; Chattopadhyay et al. 2012). Sharma & Nath (2012) showed that radiation pressure becomes important only for galaxies with mass $\geq 10^{12} M_{\odot}$ and with high SFR, e.g., for ULIRGs. However, the formation process of these clouds remain uncertain. Marcolini et al. (2005) argued that the clouds are likely to be shredded by Kelvin-Helmholtz instability and/or evaporation due to thermal conduction, with a time scale $\leq 1 \text{ Myr}$. It is therefore a puzzle that these clouds are often observed at distances of several kpc, since the travel time (assuming the speed to be a few hundred km s^{-1}) is likely to be $\sim 10 \text{ Myr}$. Nath & Silk (2009) and Murray et al. (2011) have suggested a scenario in which radiation pressure pushes a shell of gas and dust which then fragments after being accelerated by thermal pressure from SNe ejecta.

High velocity clouds: The extraplanar gas is also affected by disk ISM processes in another way. In the galactic fountain model (Shapiro & Field 1976; Bregman 1980), partially ionized gas is launched from the disk by the effect of multiple supernovae (SNe), and after travelling some distance in the halo it falls back to the disk. An important problem in this regard is that of the formation of clouds in the extraplanar gas, which are observed as either high velocity clouds (HVC) or OVI clouds. Bregman (1980) argued that HVCs could form from the condensation of galactic fountain material (but see Ferrara & Einaudi 1992). However, this idea cannot

explain the fact that observed metallicity is less than that of the disk ISM (van Woerden & Wakker 2004). This is particularly important for HVCs which are more than $\sim 5 \text{ kpc}$ away from the Milky Way disk which have low metallicity ($Z \sim 0.01-0.2Z_{\odot}$). Recently, Binney et al. (2009) have argued that thermal instability is not efficient in the moving fountain gas, and clouds are rather likely to form due to the interaction of ejected disk material with an pre-existing halo gas. However, the ejected disk material is modeled in a ballistic manner, whereas in reality the outward moving gas is more likely to move like a fluid. Wakker et al. (2005) found that OVI absorption associated with HVCs can arise from the interface between the HVC and a coronal gas. The HVCs observed to be at large distances have been suggested to be related to gas accretion by the Local Group (Blitz et al. 1999). However we note that, in the HVCs nearer than $\sim 10 \text{ kpc}$, there can be a mixture of components from Galactic ISM, the interface region with halo gas, or gas from the Local group. Thus the overall picture is tangled because of a contamination at lower heights connected with interaction of falling gas with the extended gas of galactic corona or by the flows generated by internal galactic processes.

Circumgalactic medium: The gaseous content of spiral galaxies outside the disk but within the halos of dark matter, formed and shaped by various processes of accretion and outflows, as mentioned above, is generally referred to as the circumgalactic medium (CGM). This refers to the reservoir of gas at distances $\sim 100-250 \text{ kpc}$. However, its existence, and the relation to processes near and in the disk are not yet fully understood. Although outflowing gas is observed near the disk, it is not clear how far this gas propagates, and about the nature of the interaction with pre-existing gas in the halo. It is uncertain if most of the wind material escapes the halo, or is retained in the halo, and then whether or not most of this gas eventually falls back to the disk. A large amount of hot gas in halo can potentially distort the cosmic microwave background radiation through Sunyaev-Zel'dovich effect (e.g. Majumdar et al. 2001). The low density of the CGM makes it an elusive component to observe, but recently it has been detected through absorption in the line of sight of background quasars. Tumlinson et al. (2011) detected a large amount of O VI absorbing gas, at $T \sim 10^{5.5} \text{ K}$, in galaxies with moderate SFR. However, its spatial extent and the total gas (and metal) content remains to be measured with enough accuracy that can constrain theoretical models.

In the present paper we address the question of the origin of high velocity clouds, circumgalactic material and the cold clumps in galactic winds, as a result of the interaction of a steady galactic wind with the relic halo gas distribution using 2D simulations. Our aim is to show that all these constituents of extra planar material may have a common origin, which is the interaction zone between galactic outflow and hot gas in halo.

The remainder of the paper is organised as follows. In §2 we describe our simulation set-up, including the initial and boundary conditions. In §3 we give analytical estimates for the dynamics of the interaction zone, and compare the timescales relevant for the problem. In §4 we present the results of our model runs and then in §5 we discuss our results along with the implications.

2 SIMULATION SET-UP

In this section we describe the initial and boundary conditions for our simulations. We also describe the hydrodynamic code PLUTO and physics modules included in our simulations. We end the section with a discussion of various runs and to which physical sys-

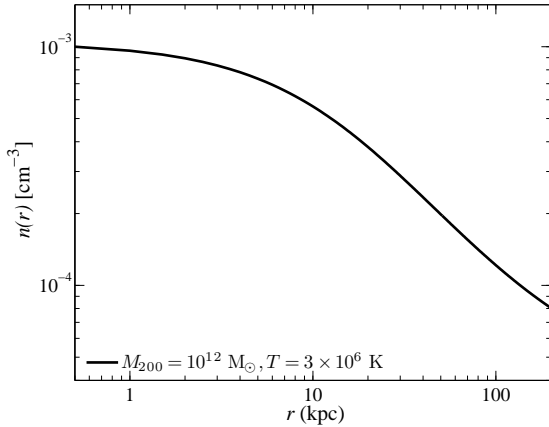


Figure 1. The density profile for the gas in the halo.

tem(galaxy) our runs resemble. In this work we use 2-D polar (r, θ) coordinate system, in which r is the radial coordinate (which relates to the in-plane distance R and height z by $r = \sqrt{R^2 + z^2}$).

The unit of density in our simulation is $1.67 \times 10^{-24} \text{ g cm}^{-3}$. Unit of velocity is 100 km s^{-1} and the unit of distance is kpc. Hence the unit of time in the present simulation is 9.5 Myr.

2.1 Initial and boundary conditions

We populate the halo with an isothermal gas distribution which is in hydrostatic equilibrium in a NFW dark matter halo. The gravitational potential for a NFW dark matter halo is given by,

$$\Phi(r) = -2v_s^2 \frac{\ln(1+r/r_s)}{r/r_s} \quad (1)$$

where $v_s^2 = GM_{200}/[2r_s f(c)]$ with $f(c) = \ln(1+c) - c/(1+c)$ and $r_s = r_{200}/c$. Here $c(= 10)$ is the halo concentration parameter, r_{200} is the virial radius and M_{200} is the virial mass. For the gravitational potential in Eq. 1, the hydrostatic density profile is given by

$$n(r) = n(r_b) \exp \left[-\frac{\mu m_p (\Phi(r) - \Phi(r_b))}{kT} \right] \quad (2)$$

where r_b is the the location of base point of wind and $\mu(= 0.6)$ is the mean molecular weight. The density at the base is $n(r_b) = 10^{-3} \text{ cm}^{-3}$. We note that the similar cored density profiles, with a central density $\sim 10^{-3} \text{ cm}^{-3}$ have been deduced for the gas in the halo of the Galaxy in recent studies (e.g. Fang et al. 2013; Putman et al. 2012; Maller & Bullock 2004). The above profile is characterised by the temperature T . We consider a temperature $T \approx 3 \times 10^6 \text{ K}$, for a milky way size halo with mass $10^{12} M_\odot$, which is roughly the virial temperature of this dark matter halo. Observations also indicate similar temperature for the hot gas in halo of the Galaxy. In Fig. 1, we have shown the density profile of the halo gas for the halo of mass $10^{12} M_\odot$, considered in this work. We set-up a simulation box in which r goes from r_b to r_{max} , and θ goes from 0 to π . Therefore the simulation box covers the upper hemisphere of galactic halo, and the spiral disc lies at the base of the hemisphere. We choose a periodic boundary condition for the θ coordinate and use the density profile given by equation 2 at the outer r boundary so that the initial hydrostatic distribution of gas does not change with time. At the lower r boundary, we also use the density profile of equation 2, except for a region where θ goes

from $\pi/2 - \alpha$ to $\pi/2 + \alpha$ (where θ is the angle with the disc plane), in which we inject the material with a specific density and velocity as we discuss below.

2.2 Injection parameters

The injection of wind gas is implemented by assuming that a supersonic wind enters the computation zone from below. We inject (continuously in time) the gas with speed v_{inj} and density n_{inj} along radial streamlines in cone with an opening angle of 2α , where $\alpha \sim 30^\circ$. The injected gas has a temperature corresponding to the sound speed (c_s) somewhat lower than the injection speed (v_{inj}) to ensure that the flow is in supersonic regime. Following Sharma & Nath (2013), this value of v_{inj} will give a wind speed $v_{\text{wind}} \sim 2v_{\text{inj}}$, which can be understood simply by the fact that in the supersonic regime, as the wind diverges, the sound speed decreases to small values and the wind speed becomes the sum of injection speed and the sound speed at the critical point at r_b . A supersonic injection from the base point r_b implies that we have assumed a spherical thermalization zone of radius r_b , centred at the galaxy in which the energy and mass injection due to stellar processes occurs. The base launching radius (r_b) in principle is a free parameter. Melioli & de Gouveia Dal Pino (2004) consider r_b in the range 100–700 pc. In the present study we work with a fixed value of $r_b = 500 \text{ pc}$. The injection speed used by us lies in the range 180–500 km s^{-1} , following the models of Sharma & Nath (2013), and corresponds to a wind speed of $v_{\text{wind}} \sim 400\text{--}1000 \text{ km s}^{-1}$.

2.3 The code and the physics included

We use the publicly available hydrodynamic code PLUTO (Mignone et al. 2007). For our runs we use the solver based on total variation diminishing Lax-Friedrich (TVDLF) scheme supplied with the code. We simulate in polar coordinates (r, θ) , with the external gravitational is due to NFW dark matter halo. PLUTO has a well tested implementation of radiative cooling (Teşileanu et al. 2008). Radiative cooling is implemented by solving the energy equation with a energy loss term, which for this study is a function of density and temperature as given by Sutherland & Dopita (1993) in case of equilibrium cooling. We assume solar metallicity for the wind and the halo gas in our simulation. The halo likely has a lower metallicity, but in this work we do not explore the effect of a two-component gas with different metallicities.

2.4 List of our runs

We have run the simulation for various values of initial and injection parameters. The quantitative details of parameters involved in our runs is provided in Table 1. We have chosen the various set of parameters to study the dependence of formation of multiphase medium on various halo gas and wind parameters.

3 ANALYTIC CONSIDERATIONS

In this section we provide analytical estimates relevant for the simulations in this work. This problem is similar to the case of a wind blown bubble where the stellar wind is expanding in a uniform density medium. The dynamics for the stellar wind blown bubble was worked out by Weaver et al. (1977). However there are some subtle differences between the stellar wind blown bubble and the present

Table 1. The parameters of our runs

| Name | $\frac{n_{inj}}{cm^{-3}}$ | $\frac{v_{inj}}{km\ s^{-1}}$ | $\frac{r_{max}}{kpc}$ | Cooling |
|------|---------------------------|------------------------------|-----------------------|---------|
| MG1 | 0.01 | 300 | 20 | No |
| MG2 | 0.01 | 300 | 20 | Yes |
| MG3 | 0.1 | 300 | 50 | Yes |
| MG4 | 0.1 | 500 | 100 | Yes |
| MG5 | 0.01 | 500 | 100 | Yes |
| MG6 | 0.002 | 300 | 20 | Yes |
| MG7 | 0.01 | 200 | 10 | Yes |
| MG8 | 0.005 | 300 | 20 | Yes |
| MG9 | 0.05 | 300 | 20 | Yes |
| MG10 | 0.1 | 400 | 100 | Yes |
| MG11 | 0.01 | 350 | 50 | Yes |
| MG12 | 0.02 | 350 | 50 | Yes |
| MG13 | 0.8 | 450 | 100 | Yes |
| MG14 | 0.005 | 500 | 100 | Yes |
| MG15 | 0.5 | 200 | 10 | Yes |
| MG16 | 1.0 | 300 | 20 | Yes |
| MG17 | 0.02 | 200 | 10 | Yes |
| MG18 | 0.05 | 200 | 10 | Yes |
| MG19 | 0.003 | 350 | 50 | Yes |
| MG20 | 0.004 | 400 | 50 | Yes |
| MG21 | 0.03 | 400 | 50 | Yes |
| MG22 | 0.03 | 500 | 100 | Yes |

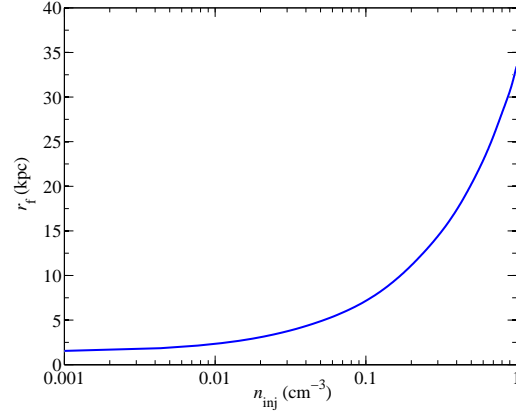
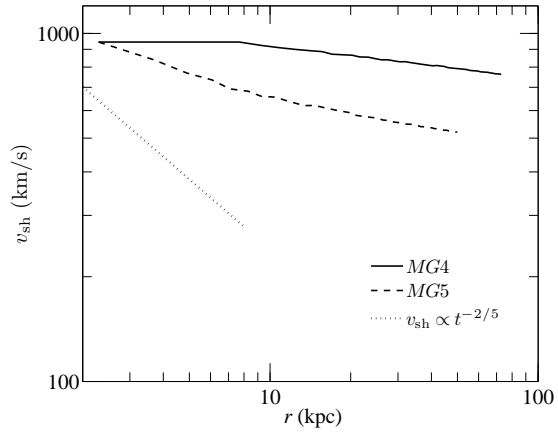
case of galactic wind interacting with the halo gas. While in the stellar wind blown bubble the ambient medium is denser than the wind, here it is the opposite, at least for the initial evolution when the wind density is larger compared to the ambient density. Also, the temperature of the ambient medium in this case is $\sim 10^6$ K, which is two orders of magnitude larger than the ISM temperature ($\sim 10^4$ K), relevant for a stellar wind blown bubble. Another difference is the stratification in the density of the ambient halo gas. Because of the stratification, the outermost shock does not slow down quickly and the late time evolution should not be given by a self-similar solution as described in Weaver et al. (1977). One should instead work out the dynamics after taking the density profile into account as in Kompaneets (1960). Due to this effect, the free expansion phase of the wind lasts longer and if the wind has enough mechanical luminosity so that it crosses the scale height of the halo gas profile, then it may keep expanding freely with the normal wind speed and eventually escape the halo. We quantify these aspects below.

In the general case of a supernova blast or a wind interacting with ambient medium there are three distinct phases of evolution. Initially there is the free expansion phase. When the swept up mass becomes comparable to the mass in the wind then the wind is obstructed by the outside mass and the free expansion phase ends and the wind enters the next phase of evolution in which the motion can be described by a self-similar solution. This phase ends when radiative losses become significant and the system enters into a momentum driven phase.

The distance (r_f) at which the transition from a free wind phase to self similar phase is expected, can be computed by equating the swept up mass with the injected mass as below,

$$\int_{r_b}^{r_f} (\Omega r^2) m_p n(r) dr = \int_0^{t_f} \Omega m_p n_{inj} v_{inj} r_b^2 dt, \quad (3)$$

where Ω is the total solid angle corresponding to wind cone, $n(r)$ is the density profile of the gas in the halo as given by equation (2) and t_f is the time which marks the end of free expansion phase. The

**Figure 2.** The extent of the free expansion phase is plotted against the wind injection density (n_{inj}) using the solid line. The value of $r_b = 0.5$ kpc.**Figure 3.** Velocity of the forward shock from our simulation runs *MG4* (solid line) and *MG5* (dashed line) is compared with the self-similar solution for a stellar wind blown bubble expanding in a uniform density ISM (dotted line).

left hand side in the above equation is the swept up mass of the halo gas and the right hand side is the total injected mass till the time t_f . The r_f is related to t_f via $r_f = \int_0^{t_f} v_{wind} dt$. As explained in the §2.2 that in the supersonic regime wind speed is, $v_{wind} \sim 2v_{inj}$, therefore $t_f = r_f / (2v_{inj})$. We have calculated the value of r_f as a function of n_{inj} which is plotted in Fig. 2 using a solid line.

In Fig. 2 we can see that r_f increases rapidly as the n_{inj} exceeds roughly $0.1\ cm^{-3}$. If the wind has enough mechanical luminosity so that it is still in the free expansion phase of evolution while it crosses the initial high density region of the halo gas, then it will keep on moving roughly with the free wind speed even at large distances as thereafter it encounters steep density gradients. Hence the self-similar phase of evolution in this case can not be described by the solution for a wind blown bubble in ISM. On the other hand if the injection density n_{inj} of the wind is small so that the free expansion phase ends well inside the high density core of the halo gas profile, then it will decelerate to smaller velocities and solution pattern is expected to resemble the Weaver et al. (1977) solution.

To illustrate this point, we plot in Figure 3 the velocities of the forward shocks from two of our simulation runs (*MG4*, *MG5*), with a higher ($n_{inj} = 0.1\ cm^{-3}$) and a low injection density ($n_{inj} = 0.01\ cm^{-3}$) respectively. We show the case of *MG4* with

a solid line and that of *MG5* with a dashed line, and compare both with the slope of $v_{\text{sh}} \propto t^{-2/5}$ (dotted line), expected for a stellar wind blown bubble expanding in a uniform density ISM. From Fig 2, the corresponding values of r_f are expected to be ~ 7 and ~ 2 kpc, respectively. Therefore the forward shock for *MG4* keeps expanding freely till ~ 7 kpc (straight part of solid line in Fig 3). While in the free expansion phase, it crosses the central core region of the halo gas density profile. After this it encounters steep density gradient, for which if we consider a power-law density profile given by $n \propto r^{-m}$, then in the self-similar phase one would expect $r_{\text{sh}} \propto t^{3/(5-m)}$ and $v_{\text{sh}} \propto t^{-(2-m)/(5-m)}$. The halo profile considered in this work beyond the core region can be approximated as a power law decrease with r , with index $m \sim 1$. One therefore expects $v_{\text{sh}} \propto t^{-0.25}$, implying only a mild decrease in velocity with time (or distance), which indeed is seen in Fig 3 for the case of *MG4* (solid line). For the case of *MG5* (dashed line), with a low injection density, the final velocity is lower because it enters the self-similar phase at the core region of the halo density profile and therefore it exhibits a steeper decrease in velocity initially.

There is one regime in which our results should resemble the self-similar solution of the ‘standard stellar wind bubble’. In an extreme situation, for very small values of r_f , the wind will decelerate quickly. We can quantify this regime in the following manner. We can see from Fig. 2 that r_f is very small for low injection densities which implies a short-lived free expansion phase. Therefore the evolution is governed mainly by the self-similar solution, for which the distance of the outermost shock is $r_{\text{sh}} = (Lt^3/\rho)^{1/5}$ and the corresponding velocity is $v_{\text{sh}} = 0.6(Lt^{-2}/\rho)^{1/5}$, where $\rho = n m_p$ is the density of the halo gas, whose value is almost constant ($\sim 10^{-3} m_p \text{ cc}^{-1}$) at small distances from the centre. Considering the inverse power law dependence of the velocity (v_{sh}) on time, it may so happen that the wind travels a small distance and it decelerates to negligible velocities. In such a case there is no significant large scale wind. Hence for very low mechanical luminosities, when n_{inj} and v_{inj} are both small, we have a small scale wind. Using the mechanical luminosity, $L = \Omega n_{\text{inj}} m_p v_{\text{inj}}^3 r_b^2$, where $\Omega = 2\pi(1 - \cos \alpha)$, is the wind cone solid angle, we can write the following general expression for r_{sh} in this case,

$$r_{\text{sh}} \sim 5 \text{ kpc} \left(\frac{n_{\text{inj}}}{0.01 \text{ cm}^{-3}} \right)^{1/2} \left(\frac{v_{\text{inj}}}{200 \text{ km/s}} \right)^{3/2} \left(\frac{v_{\text{sh}}}{50 \text{ km/s}} \right)^{-3/2}. \quad (4)$$

From the above equation, larger is the value of n_{inj} and v_{inj} , larger will be the value of r_{sh} . If we assume that the wind decelerates to a small velocity, say $v_{\text{sh}} \approx 50 \text{ km s}^{-1}$, before crossing $r_{\text{sh}} \approx 5 \text{ kpc}$, then the corresponding values of n_{inj} and v_{inj} separates the cases of standard small scale wind bubble and the large scale galactic wind.

We also note that if the n_{inj} is too large such that the total energy lost per unit time due to radiative cooling (\dot{E}_{cool}) at the base is more than the energy injection rate at the base ($\dot{E}_{\text{kin}} \sim m_p n_{\text{inj}} v_{\text{inj}}^3 4\pi r_b^2$), then it will lead to catastrophic cooling. To quantify this we can define the following ratio,

$$\frac{\dot{E}_{\text{cool}}}{\dot{E}_{\text{kin}}} \sim \frac{\left(\frac{4\pi}{3} r_b^3\right) (n_{\text{inj}})^2 \Lambda}{m_p n_{\text{inj}} v_{\text{inj}}^3 4\pi r_b^2} \sim \left(\frac{n_{\text{inj}}}{1 \text{ cm}^{-3}} \right) \left(\frac{v_{\text{inj}}}{300 \text{ km s}^{-1}} \right)^{-3}, \quad (5)$$

assuming $\Lambda \sim 10^{-22} \text{ erg cm}^3 \text{ s}^{-1}$.

4 THE SIMULATION RESULTS

Here we present the results from five of our runs. To start with we show the case with no radiative cooling in Figure 4, which clearly

demonstrates the effect of the halo gas on the wind. One can see the formation of eddies at the periphery of the wind cone due to the relative motion between the wind gas and the halo gas, and the onset of Kelvin-Helmholtz instability. This leads to turbulent mixing of gas in the halo. Note that the forward shock in this run reaches a distance of ~ 20 kpc in the vertical direction by 47 Myr, and shock heats the ambient halo gas. At this time, there is a contact discontinuity at a vertical distance of ~ 10 kpc, where one finds a slightly higher density (and therefore lower temperature, since pressure is continuous across the region). The region vertically below this contact discontinuity is occupied by shocked wind gas, and heated by the reverse shock.

If a wind is launched with a radial injection in vacuum, it diverges geometrically as it reaches large distances. In other words if the injection and the external forces are spherically symmetric then the wind will keep following the radial streamlines. However if the wind (launched in a fraction of total solid angle) is moving through an ambient medium, it may or may not diverge with increasing distance, depending on how stratified the ambient medium is. It has been shown that if the ambient medium has an exponential or Gaussian density distribution then also the wind diverges as it does in vacuum (Mac Low et al. 1989). However if the decrease in density is not steep, then one would expect a reduction in the cone width at large distances. In this first case of ours we can see in Fig. 4 that the wind cone does not diverge as much as it should have done if it were to expand freely in vacuum. Rather, at large distances the span of the wind cone becomes fixed, except in the final snapshot where rolling eddies strike the wall of the wind cone and the wind cone is somewhat squeezed. The ram pressure of the gas in the wind cone is highly anisotropic, and is dominated by motion in the (almost) vertical direction. The gas in the eddies, however, carry ram pressure in both radial and transverse directions. We have found that whenever the ram pressure of the gas in the eddies becomes comparable to the ram pressure of the the wind gas, the wind cone is disturbed and the cone is squeezed temporarily (and comes back to the original size when the effect of the eddies is gone, as we have found from extending the simulation to a longer duration).

In Figure 5, we show the density and temperature evolution for the case *MG2*, for which the injection density and velocity are the same as in previous case however radiative cooling is switched on. An additional fact which is now evident is the formation of cold fragments in the high density zones, which are the interaction zones between the halo and wind gas on the periphery of the wind cone. In this particular case ($n_{\text{inj}} = 0.01 \text{ cm}^{-3}$, $v_{\text{inj}} = 300 \text{ km s}^{-1}$), the cold clouds that form on the periphery of the eddies fall back, but the clouds that form on top of the wind cone escapes the simulation box by the end of the run. The fragments which fall back on the disk do not form only from the gas ejected from the disk, but rather from the mixed gas in the interaction zone between the wind and halo gas. Therefore in the real galactic situations, if the clouds form via this mechanism then they are likely to have a range of metallicities (considering the mixing of high metallicity wind gas with low metallicity halo gas), similar to the case of high velocity clouds in Milky Way. This therefore represents a variation on the theme of galactic fountain, but with the important difference that clouds form in the interaction between wind and halo gas. Note that the clouds fall back within the span (~ 10 kpc) of the gaseous disk.

Next, we increase the wind density and the size of the simulation box. In Figure 6 we show the case of $n_{\text{inj}} = 0.1 \text{ cm}^{-3}$ and with the same wind speed as before. The enhanced wind momentum in this case is able to plough through the halo gas more effectively,

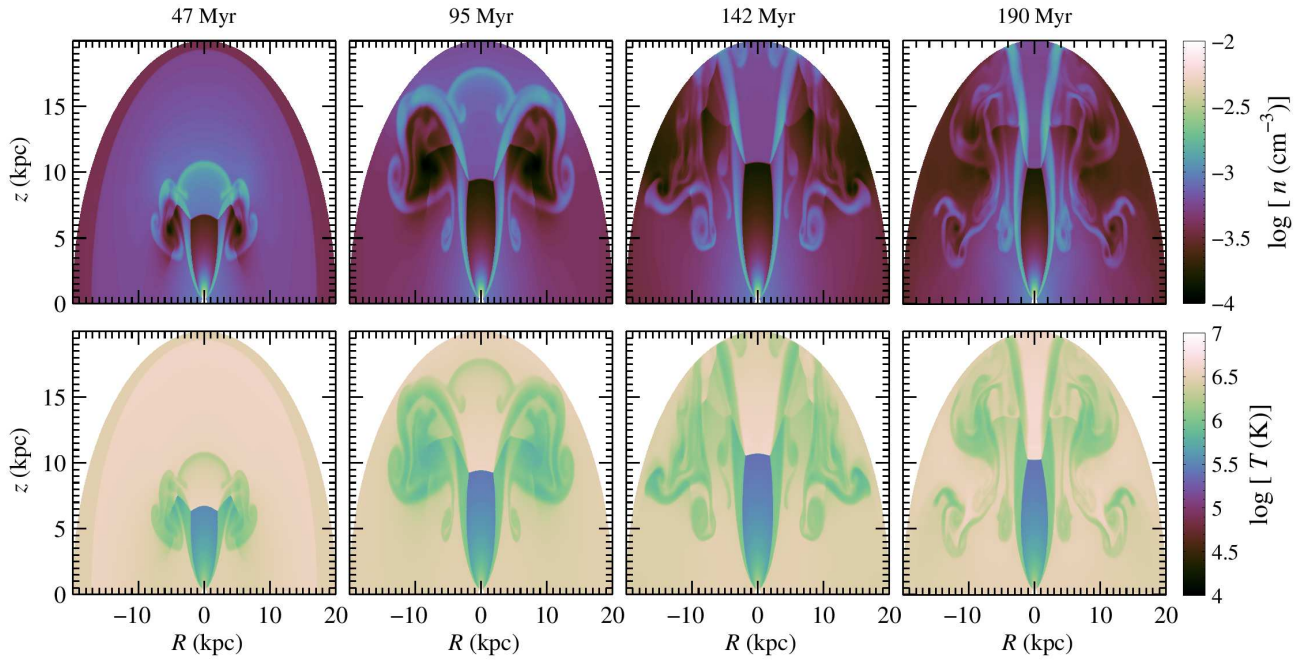


Figure 4. Time evolution of log of density (upper panel) and log of temperature (lower panel) in our first run, *MG1*, without radiative cooling. Wind injection velocity is 300 km s^{-1} .

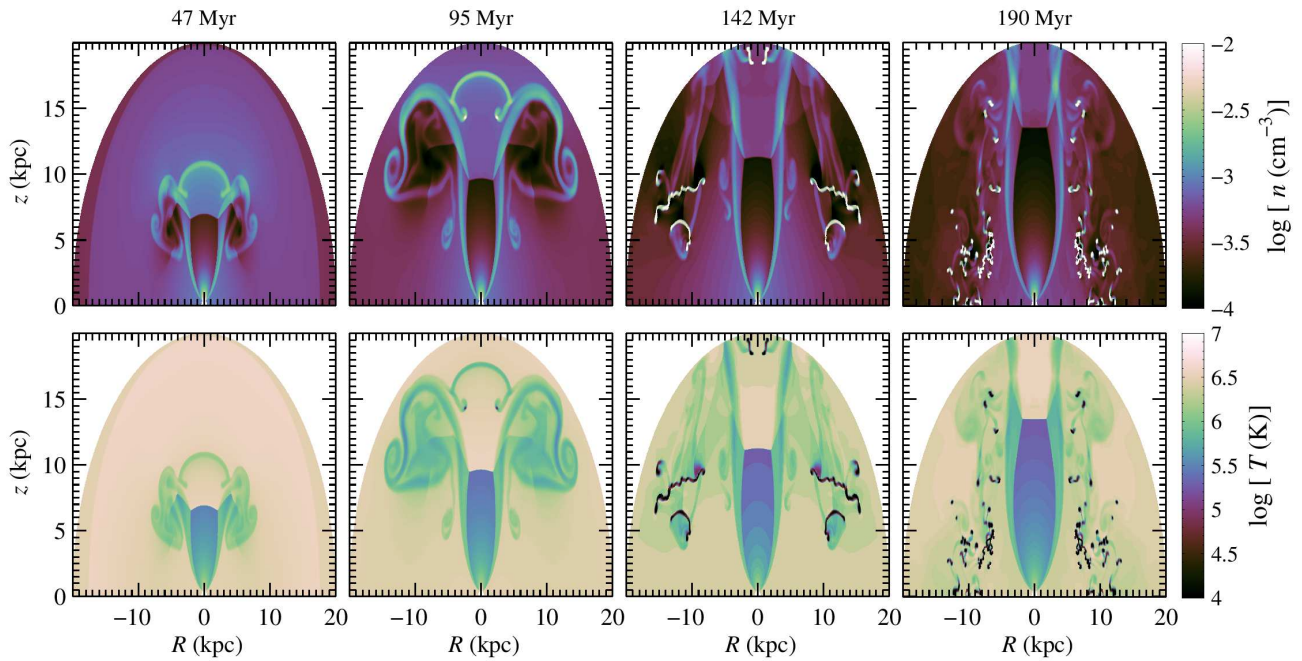


Figure 5. Time evolution of log of density (upper panel) and log of temperature (lower panel) in the run *MG2*. Wind injection velocity is 300 km s^{-1} and injection density at the base is 0.01 cm^{-3} .

as a result of which we do see a diverging wind cone (in contrast to earlier cases). In this case, we have mostly forward moving gas and even the clumps which form in the interaction zone ride with the flow in the simulation box. The clouds formed in this case represent the case of ram pressure driven clouds in superwinds. The temperature plots in this run show temperatures less than 10^4 K in the entire wind cone. This has occurred due to strong cooling in this

higher density case. This structure is an outcome of our assumption of single injection site centred at the galaxy. In reality the injection zones may be randomly distributed in the entire disc. In that case the winds emerging from different injection zones will collide and there will be a more non-uniform density and temperature profile in the region above the disc plane (e.g. Melioli et al. 2013).

In Figure 7, we increase the wind injection speed to 500 km s^{-1}

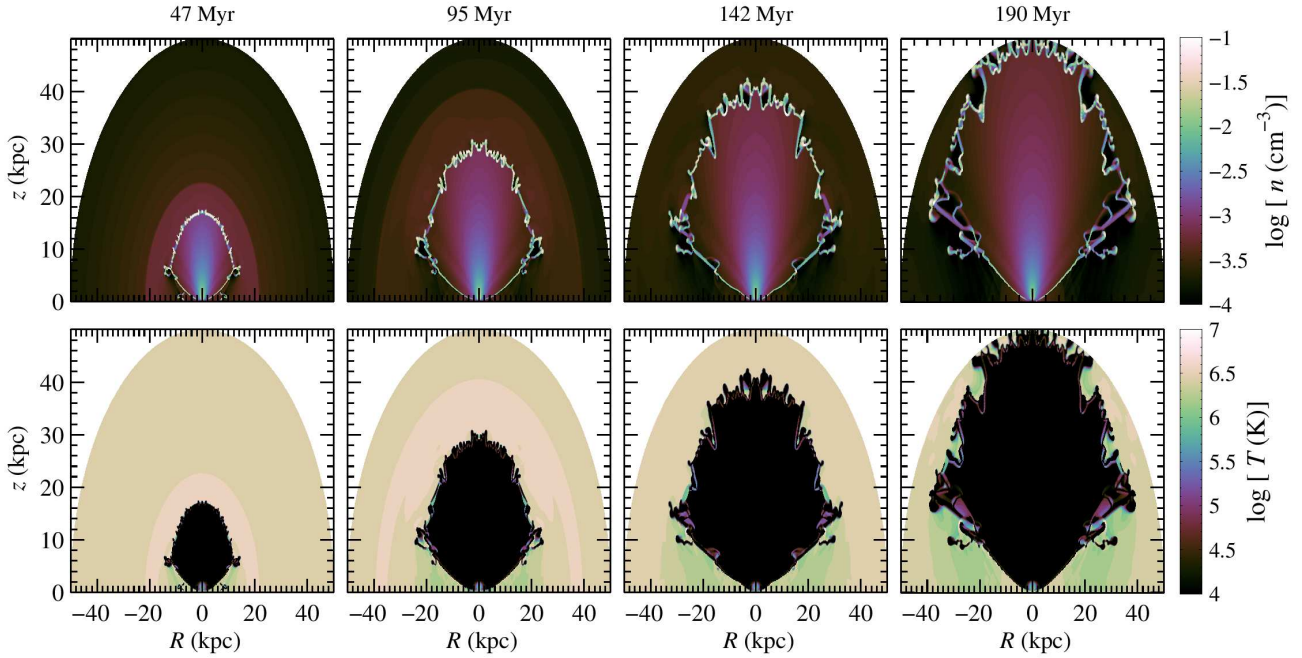


Figure 6. Time evolution of log of density (upper panel) and log of temperature (lower panel) in the run *MG3*. Wind injection velocity is 300 km s^{-1} and injection density at the base is 0.1 cm^{-3} .

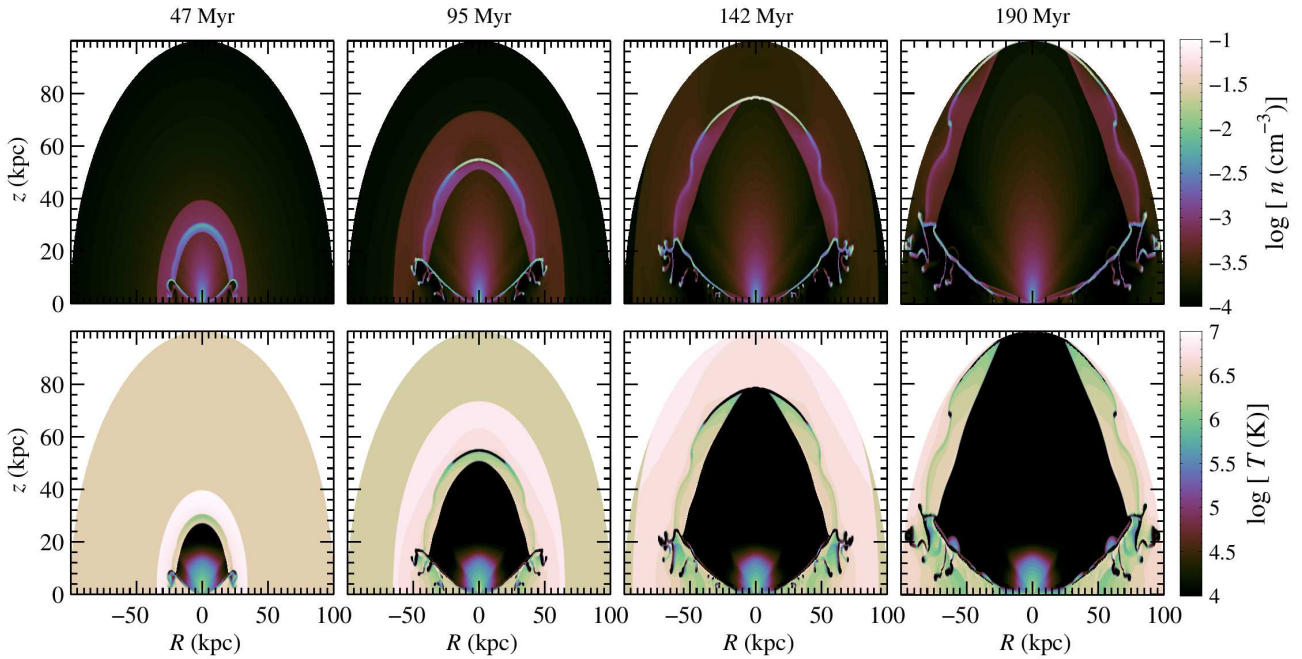


Figure 7. Time evolution of log of density (upper panel) and log of temperature (lower panel) in the run *MG4*. Wind injection velocity is 500 km s^{-1} and injection density at the base is 0.1 cm^{-3} .

s^{-1} and also the size of the simulation box, in order to study whether or not the wind with large injection speed can travel large distances and escape. In this case, the wind clears the simulation box in $\sim 200 \text{ Myr}$, including the clouds that form on the top of the wind cone. However, there is a population of clouds that form near the lower boundary of the wind cone, which appear to fall back to the mid-plane but at large distances from the gaseous disk (≥ 10

kpc). This process may be important in gas infall at large galactocentric radii and lead to the increase of disk size.

Finally, in Fig. 8 we decrease the wind density but retain the high speed and the box size from the previous run. In this case, radiative cooling is not so effective because of lower density. Also, the wind cannot escape because at some value of r the wind density falls below that of the halo gas. As a combined effect of these

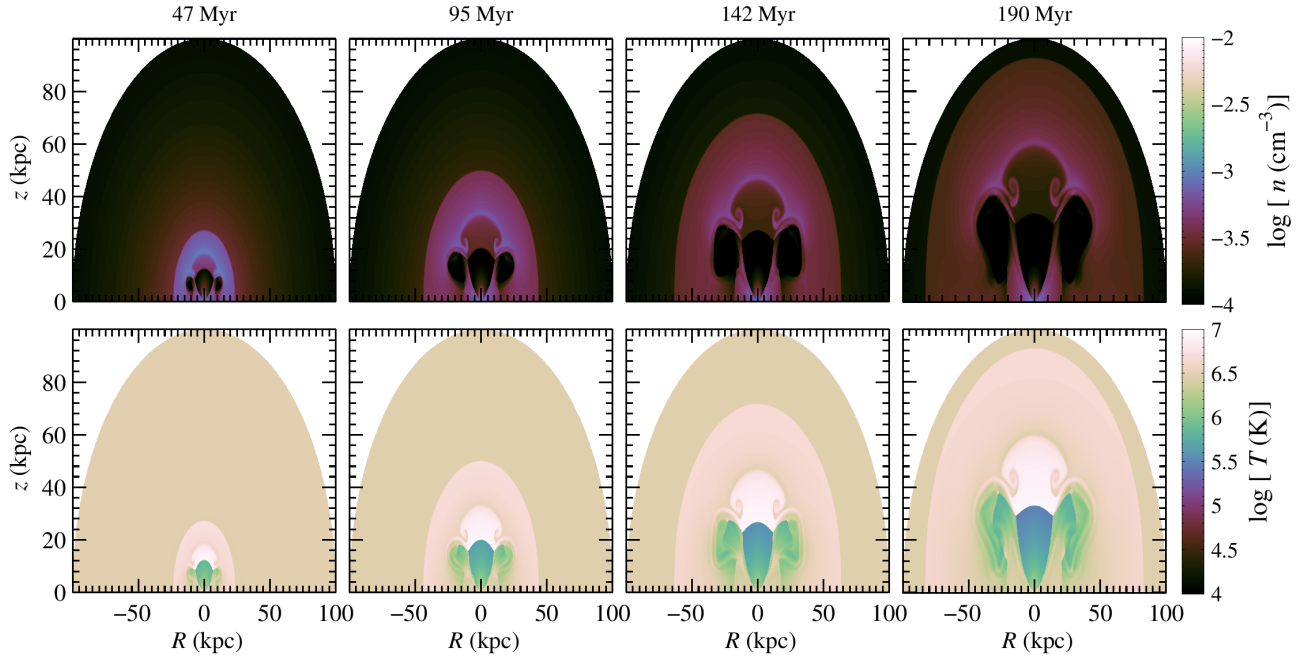


Figure 8. Time evolution of log of density (upper panel) and log of temperature (lower panel) in the run *MG5*. Wind injection velocity is 500 km s^{-1} and injection density at the base is 0.01 cm^{-3} .

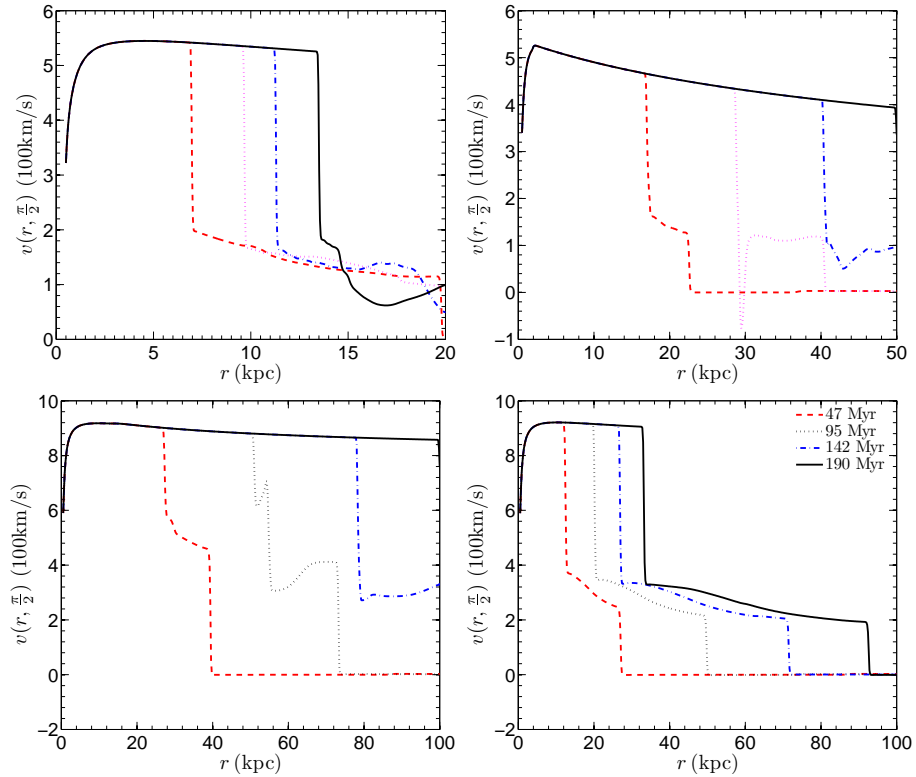


Figure 9. Velocity along the z -axis in computational box at four different times for our runs *MG2* (top-left), *MG3* (top-right), *MG4* (bottom-left) and *MG5* (bottom-right).

two aspects, we have regions of low density warm gas (10^5 – 10^6 K) present in the halo, as shown in the density and temperature snapshots. The column density of this warm gas is $\geq 10^{18}$ cm $^{-2}$, e.g. for a density of $\sim 10^{-4}$ cm $^{-3}$ and a length scale of ~ 10 kpc. Hence these regions are likely candidates for OVI absorption systems recently observed as a circum-galactic medium in the halos of galaxies (Tumlinson et al 2011).

Note that a warm-hot phase (10^5 – 10^6 K) is also present in other cases. For example if we look at the temperature profile of falling clouds in lower panel of *MG2* in Fig. 5, they have a wake of warm gas behind them, which appears greenish and roughly corresponds to a temperature of 10^{5-6} K. We note that presence of warm-hot medium in the wakes of high velocity clouds is also suggested recently by Marasco et al. (2013). Furthermore, the temperature snapshots of *MG1* (the simulation run without cooling) show regions with gas at $\sim 10^{5.5}$ K, which implies that if the cooling is suppressed (possibly in systems with low metallicities), one can also generate OVI absorption systems simply by adiabatic cooling of galactic wind gas that is confined inside the halo.

We note that the two rarefied regions on the periphery of the wind cone in *MG5* are similar to that in the case of *MG2*, which in the case of low injection speed (for *MG2*) interacts with large halo density gas and thereby fragments into cold clouds. In the case of high injection speed in *MG5*, the wind gas travels to further distances in the halo where the ambient gas density is small and therefore the interaction zone does not cool and fragment, only gets rarefied

We plot the gas velocities as a function of the vertical distance for four snapshots in the case of *MG2* (top left panel), *MG3* (top right), *MG4* (bottom left), *MG5* (bottom right) in Figure 9. The wind speed initially increases to a value almost double of the injection speed, as expected in a steady (transonic) wind case (Sharma & Nath 2013), and explained in §2.2. The wind speed then drops to a low value at a certain distance because of the interaction with halo gas. This signifies the boundary between the steady wind and shocked wind that arises due to a reverse shock. Thereafter the velocity remains constant for some segment in the shocked wind region. Then, depending on the efficiency of cooling, there is a formation of thin shell which becomes momentum driven, and a consequent rise in the velocity is seen (see, e.g., the dotted lines in top-right and bottom-left panels of Fig 8, corresponding to the snapshots at 95 Myr). In contrast, for the case of low cooling efficiency (bottom right panel, for the run *MG5*), the shocked region is thick and the existence of thin shells is not apparent in the velocity plot.

Another important point to note in the velocity plots is the effect of the halo gas in decelerating the wind front. Compare the bottom-left and bottom-right panels, for the same injection speed of 500 km s $^{-1}$. With a lower injection density in the bottom-right panel, we find that the wind is unable to escape even when the injection speed is large enough to overcome the gravitational potential barrier. This is an example in which the wind is contained within the halo due to the resistance offered by the halo gas. This aspect is also clear from our discussion in §3 where in Fig 3 we have plotted the velocities of the forward shocks for *MG4*, *MG5* using solid and dashed lines. For *MG5*, the velocity of the forward shock is almost half of that in *MG4*.

We would like to point out that the wind gas cools but does not fragment while the fragmentation occurs only in the dense shell. The reason is that thermal instability grows fast in the compressed high density region while the wind gas diverges on account of its

speed, and becomes dilute after entering the simulation box, and the low density does not favour thermal instability.

5 DISCUSSION

We summarise our results by representing the outcome of different simulation runs in the parameter space of $n_{inj} - v_{inj}$ in Figure 10. For this purpose we use the results of all of runs mentioned in Table 1, besides the ones discussed in the previous section. Based on our discussions so far, we categorise our results in following four classes and compare with analytical expectations:

- *Standard stellar wind bubble*: As discussed in the beginning of our analytical estimates (§3), if the shell decelerates to negligible speeds within a distance ~ 5 kpc, then the wind is confined to small scales and we refer to the case as standard stellar wind bubble. At later times the wind material in this case collapses on itself. We mark these cases with open circles in Fig 10.

The limiting combination of n_{inj} and v_{inj} that leads to such cases can be obtained from equation (4) by requiring $r_{sh} \leq 5$ kpc, and one finds a scaling of $v_{inj} \propto n_{inj}^{1/3}$ which divides this small scale wind with the galactic wind. We show this limiting combination as a solid line in the bottom-left corner of Fig 10.

- *Warm circum-galactic medium*: If the interaction between the wind and the halo gas leads to significant regions of warm-hot (10^5 – 10^6 K) gas, where cooling is not effective enough to produce cold clumps, then we categorise our simulation runs as having produced warm CGM. The column density of the warm-hot gas in this case is sufficiently large to explain the observed OVI absorption, as discussed earlier. We mark these cases in Fig 10 with filled circles.

For the cases shown by filled circles, the cooling is therefore not significant. We can compare the dynamical and cooling time to understand the reason behind the lack of cooling in these cases. For a compressed region of density n_{sh} , the cooling time is given by $t_{cool} \propto T_{sh}/(n_{sh}\Lambda)$, where $\Lambda \propto T_{sh}^{-1/2}$ is the cooling function for the temperature range 10^5 – 10^7 K, and $T_{sh} \propto v_{sh}^2$ is the temperature behind the forward shock. Thus the cooling time scales as $t_{cool} \propto v_{sh}^3/n_{sh}$. As the CGM material is seen in the runs which occupy mostly the low injection density region in Fig. 10 (see filled circles), therefore the dynamics of the compressed region should approximately be governed by a self-similar solution for which we can write $t \propto L^{1/2} v_{sh}^{-5/2} \propto n_{inj}^{1/2} v_{inj}^{3/2} v_{sh}^{-5/2}$. The ratio of this dynamical to cooling time is

$$\frac{t}{t_{cool}} \propto n_{sh}^{1/2} n_{inj}^{3/2} v_{sh}^{-11/2}. \quad (6)$$

The velocity of the compressed region can be written as $v_{sh} = \alpha v_{inj}$, where α ranges from 0 to 1 depending on the evolutionary stage of the shell. Considering a constant density for the compressed region n_{sh} (because it depends on ambient gas density), and setting $t = t_{cool}$, we obtain the scaling $v_{inj} \propto n_{inj}^{1/8}$. We draw a dashed line in Fig 10 for this scaling, so that the region lying on the left side of this line would have $t < t_{cool}$, implying a cooling time larger than the dynamical time. It is interesting to note that for $\alpha \sim 0.4$ which has been used to draw the dashed line, most of the filled circles (denoting the existence of CGM) do lie in this region bounded by this approximate scaling.

- *Cold clouds*: In the contrasting case of $t_{cool} < t_{sh}$, the interaction zone fragments rapidly into cold clouds of $T \sim 10^4$ K. As the wind gas ploughs through the halo gas, eddies are formed in the side walls due to the relative motion. These eddies break out of the bulk flow and as they cool, the fragments fall back to the disk. This

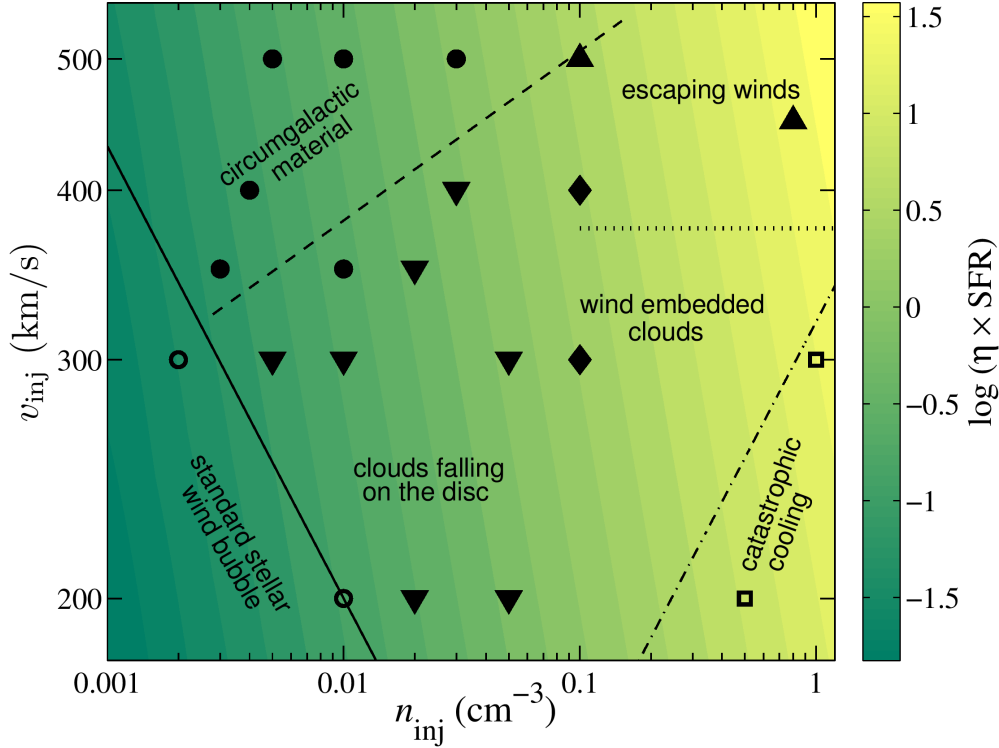


Figure 10. Simulation runs in parameter space of n_{inj} and v_{inj} . The lines represent the analytically expected power laws which divide the various regions. The quantity η SFR, which is the mass loading rate in the wind, is shown by the color coding.

represents the case of high velocity clouds if the clouds fall back within the lengthscale of the gaseous disk, and we mark these cases with triangles pointing downward in Fig 10 (e.g., *MG2*).

If the injection speed and density are high, then the wind cone region laterally extends beyond the gaseous disk (~ 10 kpc). In this case the infalling clouds fall beyond ~ 10 kpc. We mark these cases with diamonds in Fig 10 (e.g., *MG3*). However, the fragments which are formed on the top of the wind cone, are driven by the ram pressure of the steady wind in both cases (down-pointing triangles and diamonds). This represents the case of cold clouds embedded in steady winds (Sharma & Nath 2012; Murray et al. 2011).

- *Escaping outflows*: If the wind density and speed are further increased, then the wind crosses 100 kpc (our simulation box) and possibly escapes the virial radius. Two of our simulation runs show these features and are marked by triangles pointing upward in the top-right corner of Fig. 10. The shell in this case fragments as well and clumps are driven into the intergalactic medium (IGM). These cases are responsible for the metal enrichment of the IGM (Nath & Trentham 1997; Madau et al. 2001; Samui et al. 2008).

The criterion for winds to escape is given by Sharma & Nath (2013) as $v_{\text{inj}} > v_s$. For our simulation runs, $v_s = 375 \text{ km s}^{-1}$. Also, n_{inj} should be such that the wind density at ~ 100 kpc is not lower than the halo gas density at that distance. Since in the steady wind region $\rho \propto r^{-2}$, we find that escape is possible for $n_{\text{inj}} \geq 0.1 \text{ cm}^{-3}$. The region above the dotted line in Fig 10 represents the escape wind regime.

- *Catastrophic cooling*: If the injection density is very large, then the energy loss by cooling can be catastrophic and the wind material enters the simulation box and cools quickly before it can diverge into a cone. Two of our simulation runs show this characteristic and are marked by open squares in Fig 10.

The corresponding criteria for this case can be inferred from eqn 6 by setting $\dot{E}_{\text{cool}} < \dot{E}_{\text{kin}}$. The boundary line for this case has a scaling of $v_{\text{inj}} \propto \rho_{\text{inj}}^{1/3}$, and is shown in Fig 10 by a dash-dotted line.

The points and different zones marked in Fig 10 shows that the outcomes of our simulation runs are in good agreement with the analytical expectations.

The mass loading rate in the wind can be written as $\dot{M} = (\Omega r_b^2) m_p n_{\text{inj}} v_{\text{inj}}^3$, where Ω is the solid angle of the wind cone. The mass loading rate is expected to scale with the star formation rate (SFR) ($\dot{M} = \eta \text{ SFR}$). In Fig 10 we have plotted this quantity using a colour code for increasing \dot{M} from dark green to bright yellow. If we consider $\eta = 1$, then the dark green regions correspond to low SFR and the bright yellow regions, to high SFR. We can see that the simulation runs producing CGM fall mostly in the low SFR region. The escaping winds and wind embedded clouds occupy the high SFR zones, and the infalling cold clouds occupy the intermediate SFR regions. For Milky Way with a SFR $\sim 3 M_{\odot} \text{ yr}^{-1}$, and considering a low $v_{\text{wind}} = 2v_{\text{inj}}$, it should occupy the lower central region of Fig 10. The result that this region is dominated by infalling clouds in our simulations, agrees with the observations of HVCs in our Galaxy. A detailed comparison of HVCs with simulation of interaction between wind and halo gas will be addressed in a future paper.

If we assume that the initial stage of galactic evolution is marked by high SFR, then we expect those galaxies to occupy the top-right corner of Fig 10, the region of escaping winds. As the galaxy loses gas via these escaping winds, the SFR decreases, and one enters the regions of either to the left or bottom-left of Fig 9 depending on the rate of decrement of SFR. This will determine

whether or not these galaxies should have a significant amount of CGM or infalling clouds (which may sustain the SFR). Therefore the interaction between the wind and the halo gas is a crucial factor in galactic evolution.

Acknowledgement: The authors acknowledge support from an Indo-Russian project (RFBR grant 08-02-91321, DST-India grant INT-RFBR-P121).

REFERENCES

- Anderson M. E., Bregman J. N., 2010, *ApJ*, 714, 320
 Binney J., 1977, *ApJ*, 215, 483
 Binney J., Nipoti C., Fraternali F., 2009, *MNRAS*, 397, 1804
 Birnboim Y., Dekel A., 2003, *MNRAS*, 345, 349
 Blitz L., Spergel D. N., Teuben P. J., Hartmann D., Burton W. B., 1999, *ApJ*, 514, 818
 Bregman J. N., 1980, *ApJ*, 236, 577
 Burke J. A., 1968, *MNRAS*, 140, 241
 Chattopadhyay I., Sharma M., Nath B. B., Ryu D., 2012, *MNRAS*, 423, 2153
 Chevalier R. A., Clegg A. W., 1985, *Nature*, 317, 44
 Fang T., Bullock J., Boylan-Kolchin M., 2013, *ApJ*, 762, 20
 Ferrara A., Einaudi G., 1992, *ApJ*, 395, 475
 Fukugita M., Hogan C. J., Peebles P. J. E., 1998, *ApJ*, 503, 518
 Johnson H. E., Axford W. I., 1971, *ApJ*, 165, 381
 Kauffmann G., Heckman T. M., De Lucia G., Brinchmann J., Charlot S., Tremonti C., White S. D. M., Brinkmann J., 2006, *MNRAS*, 367, 1394
 Kompaneets A. S., 1960, *Soviet Physics Doklady*, 5, 46
 Mac Low M.-M., Ferrara A., 1999, *ApJ*, 513, 142
 Mac Low M.-M., McCray R., Norman M. L., 1989, *ApJ*, 337, 141
 Madau P., Ferrara A., Rees M. J., 2001, *ApJ*, 555, 92
 Majumdar S., Nath B. B., Chiba M., 2001, *MNRAS*, 324, 537
 Maller A. H., Bullock J. S., 2004, *MNRAS*, 355, 694
 Marasco A., Marinacci F., Fraternali F., 2013, *ArXiv*: 1305.2964
 Marcolini A., Strickland D. K., D’Ercole A., Heckman T. M., Hoopes C. G., 2005, *MNRAS*, 362, 626
 Martin C. L., 2005, *ApJ*, 621, 227
 Melioli C., de Gouveia Dal Pino E. M., 2004, *A&A*, 424, 817
 Melioli C., de Gouveia Dal Pino E. M., Geraissate F. G., 2013, *MNRAS*, 430, 3235
 Mignone A., Bodo G., Massaglia S., Matsakos T., Tesileanu O., Zanni C., Ferrari A., 2007, *ApJS*, 170, 228
 Murray N., Ménard B., Thompson T. A., 2011, *ApJ*, 735, 66
 Murray N., Quataert E., Thompson T. A., 2005, *ApJ*, 618, 569
 Nath B. B., Silk J., 2009, *MNRAS*, 396, L90
 Nath B. B., Trentham N., 1997, *MNRAS*, 291, 505
 Navarro J. F., Frenk C. S., White S. D. M., 1997, *ApJ*, 490, 493
 Pickelner S. B., Shklovsky I. S., 1958, *Rev. Mod. Phys.*, 30, 935
 Putman M. E., Peek J. E. G., Joung M. R., 2012, *ARA&A*, 50, 491
 Rasmussen J., Sommer-Larsen J., Pedersen K., Toft S., Benson A., Bower R. G., Grove L. F., 2009, *ApJ*, 697, 79
 Rossa J., Dettmar R.-J., Walterbos R. A. M., Norman C. A., 2004, *AJ*, 128, 674
 Samui S., Subramanian K., Srianand R., 2008, *MNRAS*, 385, 783
 Shapiro P. R., Field G. B., 1976, *ApJ*, 205, 762
 Sharma M., Nath B. B., 2012, *ApJ*, 750, 55
 Sharma M., Nath B. B., 2013, *ApJ*, 763, 17
 Sharma M., Nath B. B., Shchekinov Y., 2011, *ApJ*, 736, L27
 Silk J., 1977, *ApJ*, 211, 638
 Spitzer, Jr. L., 1956, *ApJ*, 124, 20
 Strickland D. K., Heckman T. M., Colbert E. J. M., Hoopes C. G., Weaver K. A., 2004, *ApJS*, 151, 193
 Suchkov A. A., Balsara D. S., Heckman T. M., Leitherer C., 1994, *ApJ*, 430, 511
 Sutherland R. S., Dopita M. A., 1993, *ApJS*, 88, 253
 Swaters R. A., Sancisi R., van der Hulst J. M., 1997, *ApJ*, 491, 140
 Teşileanu O., Mignone A., Massaglia S., 2008, *A&A*, 488, 429
 Tumlinson J. et al., 2011, *Science*, 334, 948
 van Woerden H., Wakker B. P., 2004, in *Astrophysics and Space Science Library*, Vol. 312, High Velocity Clouds, van Woerden H., Wakker B. P., Schwarz U. J., de Boer K. S., eds., p. 195
 Veilleux S., Rupke D. S. N., Swaters R., 2009, *ApJ*, 700, L149
 Voigtländer P., Kamphuis P., Marcelin M., Bomans D. J., Dettmar R.-J., 2013, *ArXiv e-prints*
 Wakker B. P., Savage B. D., Sembach K. R., Richter P., Fox A. J., 2005, in *Astronomical Society of the Pacific Conference Series*, Vol. 331, Extra-Planar Gas, Braun R., ed., p. 11
 Wang B., 1995, *ApJ*, 444, 590
 Wang Q. D., 2001, in *Astronomical Society of the Pacific Conference Series*, Vol. 230, Galaxy Disks and Disk Galaxies, Funes J. G., Corsini E. M., eds., pp. 393–396
 Wang Q. D., 2007, in *EAS Publications Series*, Vol. 24, EAS Publications Series, Emsellem E., Wozniak H., Massarier G., Gonzalez J.-F., Devriendt J., Champavert N., eds., pp. 59–72
 Weaver R., McCray R., Castor J., Shapiro P., Moore R., 1977, *ApJ*, 218, 377
 White S. D. M., Frenk C. S., 1991, *ApJ*, 379, 52
 White S. D. M., Rees M. J., 1978, *MNRAS*, 183, 341